

# Protein quality control at the inner nuclear membrane

Anton Khmelinskii<sup>1\*</sup>, Ewa Blaszcak<sup>2,3\*</sup>, Marina Pantazopoulou<sup>4</sup>, Bernd Fischer<sup>5,6</sup>, Deike J. Omrus<sup>4</sup>, Gaëlle Le Dez<sup>2,3</sup>, Audrey Brossard<sup>2,3</sup>, Alexander Gunnarsson<sup>4</sup>, Joseph D. Barry<sup>5</sup>, Matthias Meurer<sup>1</sup>, Daniel Kirrmaier<sup>1</sup>, Charles Boone<sup>7</sup>, Wolfgang Huber<sup>5</sup>, Gwenaël Rabut<sup>2,3</sup>, Per O. Ljungdahl<sup>4</sup> & Michael Knop<sup>1,8</sup>

The nuclear envelope is a double membrane that separates the nucleus from the cytoplasm. The inner nuclear membrane (INM) functions in essential nuclear processes including chromatin organization and regulation of gene expression<sup>1</sup>. The outer nuclear membrane is continuous with the endoplasmic reticulum and is the site of membrane protein synthesis. Protein homeostasis in this compartment is ensured by endoplasmic-reticulum-associated protein degradation (ERAD) pathways that in yeast involve the integral membrane E3 ubiquitin ligases Hrd1 and Doa10 operating with the E2 ubiquitin-conjugating enzymes Ubc6 and Ubc7 (refs 2, 3). However, little is known about protein quality control at the INM. Here we describe a protein degradation pathway at the INM in yeast (*Saccharomyces cerevisiae*) mediated by the Asi complex consisting of the RING domain proteins Asi1 and Asi3 (ref. 4). We report that the Asi complex functions together with the ubiquitin-conjugating enzymes Ubc6 and Ubc7 to degrade soluble and integral membrane proteins. Genetic evidence suggests that the Asi ubiquitin ligase defines a pathway distinct from, but complementary to, ERAD. Using unbiased screening with a novel genome-wide yeast library based on a tandem fluorescent protein timer<sup>5</sup>, we identify more than 50 substrates of the Asi, Hrd1 and Doa10 E3 ubiquitin ligases. We show that the Asi ubiquitin ligase is involved in degradation of mislocalized integral membrane proteins, thus acting to maintain and safeguard the identity of the INM.

To identify components of INM quality control, we focused on the ubiquitin-conjugating enzyme Ubc6. Ubc6 is an integral membrane protein that localizes to the endoplasmic reticulum and the INM where it targets for degradation soluble and integral membrane proteins together with Ubc7 and Doa10 (refs 6, 7). We established a microscopy-based bimolecular fluorescence complementation (BiFC) assay<sup>8</sup> to screen for new E3 ubiquitin ligases interacting with Ubc6 (Fig. 1a). In total, 10 out of 54 known or putative E3s, including Doa10, interacted with Ubc6 at distinct subcellular locations (Fig. 1b and Extended Data Fig. 1a). Among these, Asi1 and Asi3 displayed a BiFC signal restricted to the nuclear rim (Fig. 1b). Despite their colocalization at the endoplasmic reticulum, no interaction was detected between Ubc6 and Hrd1 (Extended Data Fig. 1a), suggesting a low rate of false-positive interactions in our BiFC assay.

Asi1 and Asi3 are integral membrane RING domain proteins of the INM and form the Asi complex<sup>4,9,10</sup>. Together with the INM protein Asi2, the Asi complex functions in the Ssy1-Ptr3-Ssy5 (SPS) amino-acid-sensing pathway, where it is involved in the degradation of Stp1 and Stp2 transcription factors<sup>11</sup>. We tested the interactions of Asi1 and Asi3 with all E2 ubiquitin-conjugating enzymes using the BiFC assay. In addition to Ubc6, Asi1 and Asi3 interacted with Ubc7 and weakly

with Ubc4 (Extended Data Fig. 1b-d). We validated these interactions in microscale thermophoresis experiments<sup>12</sup> with recombinant proteins (Fig. 1c and Extended Data Fig. 1e). The Ubc7-binding region of Cue1 (Cue1<sup>U7BR</sup>)<sup>13</sup>, a protein that tethers Ubc7 to the endoplasmic reticulum membrane<sup>14</sup>, was included in the assays. A carboxy-terminal fragment of Hrd1 (Hrd1<sup>CT</sup>) expected to interact with Ubc7 but not Ubc6 served as control<sup>2,3</sup>. The RING domains of Asi1 and Asi3 (Asi1<sup>RING</sup> and Asi3<sup>RING</sup>) interacted with Ubc7, provided it was bound to Cue1<sup>U7BR</sup>, with affinities similar to Hrd1<sup>CT</sup>. Asi1<sup>RING</sup> and Asi3<sup>RING</sup>, but not Hrd1<sup>CT</sup>, also interacted weakly with Ubc6 lacking its transmembrane domain (Ubc6<sup>ΔTM</sup>) (Fig. 1c).

The Asi proteins maintain the SPS pathway in the ‘off state’ in the absence of inducing amino acids, and do so by targeting for proteasomal degradation the low levels of Stp1 and Stp2 that inadvertently mislocalize into the nucleus<sup>11</sup>. Consequently, *asi* mutants exhibit aberrant constitutive Stp1/Stp2-dependent transcription<sup>9</sup>. We observed that *ubc7Δ* and, to a lesser extent, *ubc6Δ* mutants exhibited increased expression of Stp1/Stp2-regulated genes similar to the *asi1Δ* and *asi3Δ* mutants (Fig. 1d and Extended Data Fig. 1f). These effects were not due to inactivation of Hrd1 or Doa10 ubiquitin ligases (Extended Data Fig. 1f), thus implicating Ubc6 and Ubc7 in the SPS pathway.

Next, we assayed the ubiquitylation of an artificial Asi substrate based on the first 45 amino acids of Stp2 (Stp2<sup>N</sup>). This fragment of Stp2 contains a degron that is recognized by the Asi complex<sup>11</sup>. Ubiquitylation of Stp2<sup>N</sup> fused to the tandem affinity purification (TAP) tag was reduced in *ubc6Δ* and severely impaired in *asi3Δ* and *ubc7Δ* mutants (Fig. 1e). In addition, ubiquitylation of Stp1 and Stp2 mutants with constitutive SPS-independent nuclear localization was impaired in *asi1Δ* and *asi3Δ* strains (Extended Data Fig. 1g). Together, these results establish the Asi complex as an E3 ubiquitin ligase of the INM that functions with Ubc6 and Ubc7.

Functionally related genes can be identified by similarity of genetic interaction profiles<sup>15</sup>. We searched for novel functions of the Asi ubiquitin ligase by mining a genome-scale genetic interaction map<sup>16</sup>. In this data set, the fitness of 5.4 million double-mutant combinations was measured by colony size, generating genetic interaction profiles for ~75% of all *S. cerevisiae* genes. We calculated correlation coefficients between genetic interaction profiles of *ASI* genes and the other 4,458 genes in the genetic interaction map. In this analysis, the genetic interaction profiles of *ASI* genes correlated with each other and, to a similar extent, with *HRD1*, *DOA10*, *UBC6*, *UBC7* and *CUE1* among others (Fig. 2a and Supplementary Table 1), suggesting that Asi and ERAD E3 ubiquitin ligases are functionally related. We sought to determine whether they work in the same or parallel pathways. Strains lacking *HRD1* and

<sup>1</sup>Zentrum für Molekulare Biologie der Universität Heidelberg (ZMBH), DKFZ-ZMBH Alliance, Im Neuenheimer Feld 282, 69120 Heidelberg, Germany. <sup>2</sup>Centre National de la Recherche Scientifique, UMR 6290, 35000 Rennes, France. <sup>3</sup>Institut de Génétique et Développement de Rennes, Université de Rennes 1, 35000 Rennes, France. <sup>4</sup>Department of Molecular Biosciences, The Wenner-Gren Institute, Stockholm University, Svante Arrhenius väg 20B, SE-106 91 Stockholm, Sweden. <sup>5</sup>Genome Biology Unit, European Molecular Biology Laboratory (EMBL), Meyerhofstraße 1, 69117 Heidelberg, Germany. <sup>6</sup>Computational Genome Biology, German Cancer Research Center (DKFZ), Im Neuenheimer Feld 580, 69120 Heidelberg, Germany. <sup>7</sup>Department of Molecular Genetics, Donnelly Centre for Cellular and Biomolecular Research, University of Toronto, 160 College St, Toronto, Ontario M5S 3E1, Canada. <sup>8</sup>Cell Morphogenesis and Signal Transduction, German Cancer Research Center (DKFZ), Im Neuenheimer Feld 280, 69120 Heidelberg, Germany.

\*These authors contributed equally to this work.

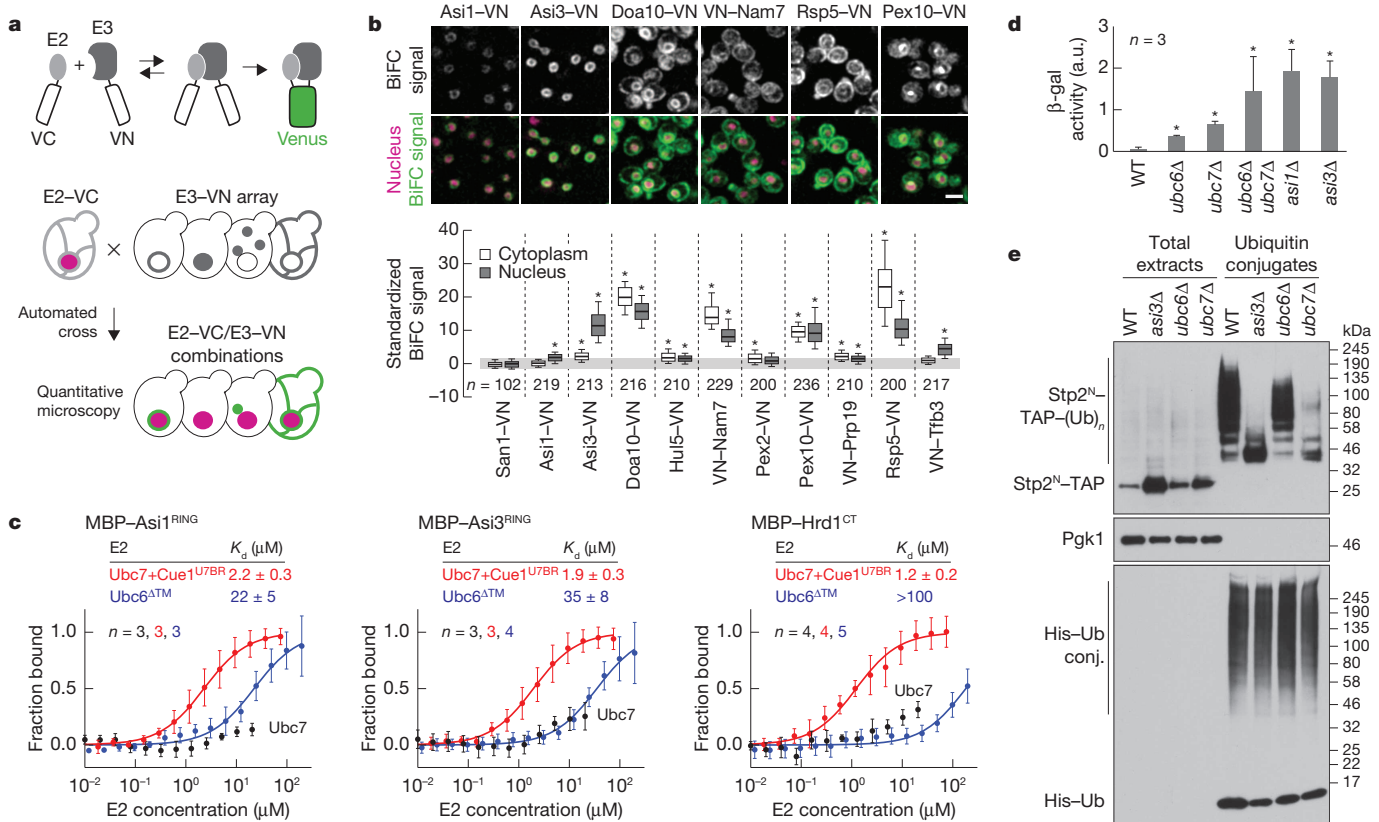


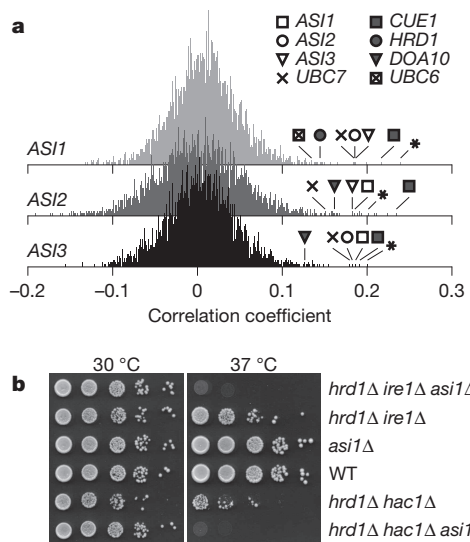
**Figure 1 |** The Asi complex is a Ubc6/Ubc7-dependent E3 ubiquitin ligase of the INM. **a**, BiFC strategy used to assay E2–E3 interactions. E2 and E3 proteins were endogenously tagged with carboxy- and amino-terminal fragments of the Venus fluorescent protein (VC and VN, respectively). Interactions between E2 and E3 proteins enable reconstitution of functional Venus that is detected with fluorescence microscopy. Rpn7 fused to the red fluorescent protein tDimer2 served as a nuclear marker. **b**, Quantification of BiFC signals in cells co-expressing VC–Ubc6 and VN-tagged E3s. Fluorescence microscopy examples representative of six fields of view (top). Scale bar, 5  $\mu$ m. BiFC signals were measured in the cytoplasm and nucleus of individual cells (bottom,  $n$  as shown). Whiskers extend from the tenth to ninetieth percentiles. **c**, Microscale thermophoresis analysis of interactions between recombinant maltose binding protein (MBP)–E3 fragments and the indicated E2s. Plots show the

fraction of MBP–E3 bound to the E2 at each tested E2 concentration (mean  $\pm$  s.d.,  $n$  as shown). Dissociation constants ( $K_d$ , mean  $\pm$  s.d.) were derived from nonlinear fits with the law of mass action (solid lines). **d**, Activity of  $\beta$ -galactosidase ( $\beta$ -gal) expressed from the *AGP1* promoter in the indicated strains (mean  $\pm$  s.d.,  $n$  = 3 clones). a.u., arbitrary units; WT, wild type. **e**, Ubiquitylation of Stp2<sup>N</sup>–TAP in strains expressing 10 $\times$ histidine (His)-tagged ubiquitin. Total cell extracts and ubiquitin conjugates eluted after immobilized-metal affinity chromatography were separated by SDS–PAGE followed by immunoblotting with antibodies against the TAP tag, Pgk1 and ubiquitin. Representative immunoblots from three technical replicates.  $*P < 10^{-4}$  (**b**; one-way analysis of variance (ANOVA) with Bonferroni correction for multiple testing) and  $*P < 0.05$  (**d**; two-tailed  $t$ -test).

the unfolded protein response genes *IRE1* or *HAC1* show impaired growth at increased temperature<sup>17</sup>. Additional deletion of *AS1* resulted in a synthetic lethal phenotype under these conditions<sup>18</sup> (Fig. 2b and Extended Data Fig. 2), suggesting that Asi1 and Hrd1 function in parallel pathways.

We used a tandem fluorescent protein timer (tFT) approach<sup>5</sup> to perform unbiased proteome-wide screens for substrates of the Asi, Hrd1 and Doa10 ubiquitin ligases. A tFT is a tag composed of two fluorescent proteins (mCherry and superfolder green fluorescent protein (sfGFP)) with distinct fluorophore maturation rates. The mCherry/sfGFP intensity ratio is a measure of protein degradation kinetics in steady state (Fig. 3a), with a dynamic range and sensitivity that exceed conventional cycloheximide chase experiments<sup>5</sup> (Supplementary Note 1). We constructed a genome-wide library of yeast strains each expressing a different tFT-tagged protein (Supplementary Methods). Library construction relied on a seamless tagging strategy that minimizes the influence of the tag on gene expression<sup>19</sup> (Extended Data Fig. 3a). In total, 4,044 proteins were successfully tagged to create a tFT library covering  $\sim$ 73% of verified or uncharacterized open reading frames in the *S. cerevisiae* genome (Supplementary Table 2). We introduced *asi1* $\Delta$ , *asi3* $\Delta$ , *hrd1* $\Delta$ , *doa10* $\Delta$ , *ubc6* $\Delta$  and *ubc7* $\Delta$  deletion alleles into the tFT library using high-throughput genetic crosses<sup>20</sup>. The effect of each gene deletion on the stability of each protein in the library was examined with high-throughput fluorescence measurements of colonies<sup>5</sup> (Extended Data Fig. 3b) and quantified as a

z-score. More proteins were stabilized (positive z-score) than destabilized in the six mutants (Extended Data Fig. 3c and Supplementary Table 3), in agreement with the role of Asi, Hrd1 and Doa10 ubiquitin ligases in protein degradation. Hierarchical clustering of top hits recapitulated known E2–E3 interactions and revealed three clusters of 20, 30 and 9 potential substrates for the Asi, Hrd1 and Doa10 ubiquitin ligases, respectively (Fig. 3b). Hrd1 substrates, including the known substrate Der1 (ref. 21), were stabilized only in the *ubc7* $\Delta$  mutant, whereas Doa10 substrates were stabilized in both *ubc6* $\Delta$  and *ubc7* $\Delta$  mutants. Most Asi substrates, including the recently identified Erg11 (ref. 18), were stabilized in the *ubc7* $\Delta$  mutant with only weak effects of the *ubc6* $\Delta$  mutant (Fig. 3b). Stp1 and Stp2 were not identified as Asi substrates in the screen, probably the consequence of their efficient targeting for degradation by the E3 ubiquitin ligase SCF<sup>Grr1</sup> in the cytoplasm<sup>11</sup>. The vast majority of potential substrates in each set were integral membrane or secretory proteins distributed along the endomembrane system and the Hrd1 and Asi substrates were enriched in endoplasmic reticulum and vacuolar proteins (Fig. 3c, d and Extended Data Fig. 3d, e). These findings are consistent with the organization and functions of endoplasmic–reticulum-associated ubiquitin ligases, thus establishing the tFT library as a valuable resource for studies of protein degradation (Supplementary Note 2), and indicate that the Asi complex is involved in degradation of a distinct set of integral membrane proteins.



We analysed this novel function of the Asi ubiquitin ligase with ten tFT-tagged substrates. Genetic crosses with additional deletion mutants revealed the involvement of Cue1 in Asi-dependent degradation (Extended Data Fig. 4a), in agreement with our biochemical analysis (Fig. 1c).

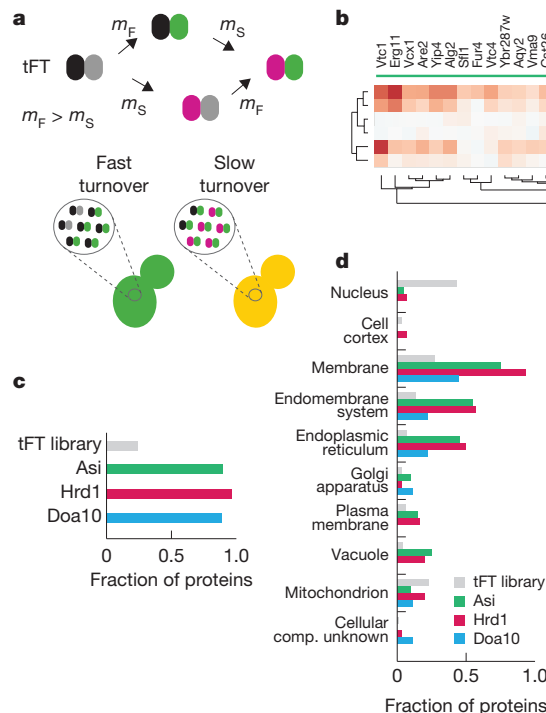
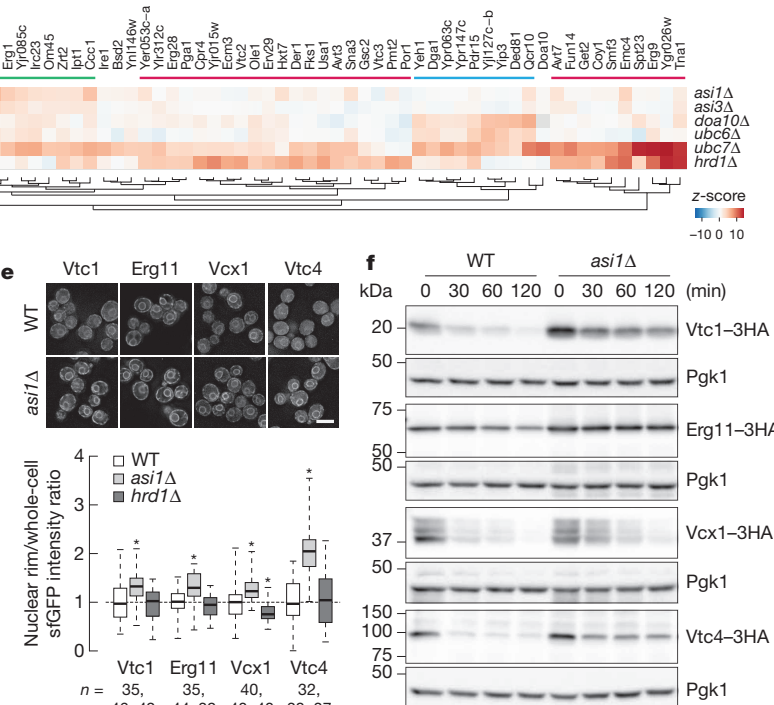


**Figure 3 | Systematic identification of substrates for Asi and ERAD E3 ubiquitin ligases.** **a**, A tandem fluorescent protein timer (tFT) is composed of two fluorescent proteins: one more slowly maturing (for example, the red fluorescent protein mCherry, maturation rate constant  $m_S$ ) and the other faster maturing (for example, the green fluorescent protein sfGFP, maturation rate constant  $m_F$ ). When fused to a protein of interest, a tFT reports on the degradation kinetics of the fusion protein: whereas fusions undergoing fast turnover are degraded before mCherry maturation, resulting in a low mCherry/sfGFP intensity ratio, the relative fraction of mature mCherry increases for proteins with slower turnover. **b**, Summary heat map of the screens for tFT-tagged proteins with altered stability in the indicated mutants. Changes in protein stability ( $z$ -score) are colour-coded from blue (decrease) to red (increase). Only proteins with a significant change in stability in at least one mutant (1% false discovery rate and  $z$ -score  $> 4$ ) are shown. Clusters of potential substrates of Asi (green), Hrd1 (red) and Doa10 (blue) E3 ubiquitin ligases are indicated. **c, d**, Fraction of proteins in the tFT library and in the three

**Figure 2 | Functional overlap between Asi and ERAD E3 ubiquitin ligases.** **a**, Histograms of Pearson correlation coefficients calculated between the genetic interaction profiles of each ASI gene and  $\sim 75\%$  of all yeast genes, obtained from a previously published genome-scale genetic interaction map<sup>16</sup>. Asterisks mark the dubious open reading frame YMR119W-A, which overlaps with the ASI1 gene. **b**, Tenfold serial dilutions of strains grown on synthetic complete medium for 2 days at 30 or 37 °C.

Several Asi substrates that were reproducibly stabilized in *asi1Δ* and *asi3Δ* mutants were not stabilized in strains lacking *ASI2* (Extended Data Fig. 4a), suggesting that *ASI2* might function as a substrate-specific recognition factor. The *ASI2*-independent nature of the interaction between *ASI3* and *Ubc6* further supports this notion (Extended Data Fig. 4b). With the exception of *Aqy2*, which was not expressed during exponential growth in liquid medium, all tFT-tagged substrates localized to the endoplasmic reticulum in wild-type cells and eight of them accumulated at the nuclear rim specifically in the *asi1Δ* mutant (Fig. 3e and Extended Data Fig. 4c). This result is consistent with protein stabilization at the INM where the Asi proteins reside. Cycloheximide chase experiments with haemagglutinin epitope (HA)-tagged variants revealed substantial turnover of *Vtc1*, *Erg11*, *Vcx1* and *Vtc4* in wild-type cells. All four proteins were stabilized specifically in the absence of *ASI1* (Fig. 3f and Extended Data Fig. 5), further validating our screening approach (Supplementary Note 1). Interestingly, *Vtc1* and *Vtc4* were previously shown to localize to the vacuolar membrane<sup>22</sup>. Both



clusters in **b** with a predicted transmembrane domain or signal peptide (**c**) or mapped to component Gene Ontology (GO) terms (**d**). Each cluster is significantly enriched in proteins with a predicted transmembrane domain or signal peptide compared to the tFT library ( $P < 2.2 \times 10^{-16}$ , Fisher's exact test). **e**, Quantification of sfGFP signals in strains expressing tFT-tagged proteins from the Asi cluster in **b**. Fluorescence microscopy examples representative of five fields of view (top). Scale bar, 5  $\mu$ m. sfGFP intensities were measured in individual cells and at the nuclear rim (bottom,  $n$  as shown). For each protein, measurements were normalized to the mean of the respective wild type. Whiskers extend from minimum to maximum values. \* $P < 0.05$  (two-tailed *t*-test). **f**, Degradation of 3 $\times$ HA-tagged proteins after blocking translation with cycloheximide. Whole-cell extracts were separated by SDS-PAGE followed by immunoblotting with antibodies against the HA tag and Pgk1 as loading control. Representative immunoblots from three technical replicates.

proteins mislocalize to the endoplasmic reticulum and nuclear rim only on overexpression or C-terminal tagging (Extended Data Fig. 6). Whether the Asi ubiquitin ligase recognizes such mislocalized proteins through specific degrons, as is the case with Stp1 and Stp2 transcription factors<sup>11</sup>, or other features such as compartment-specific properties of transmembrane domains<sup>23</sup> is an open question.

The nuclear pore complex establishes a barrier between the cytoplasm and the nucleoplasm. However, increasing evidence suggests that not only small soluble proteins but also integral membrane proteins with cytoplasmic domains of up to 60 kilodaltons (kDa) can passively diffuse past the nuclear pore, the latter through a ~10 nm side channel<sup>6,24–28</sup>. We propose that the Asi ubiquitin ligase targets such mislocalized and potentially harmful proteins for degradation. Although the Asi proteins are not obviously conserved outside of yeast, the general importance of membrane-associated protein degradation mechanisms and the large diversity of integral membrane RING domain proteins in mammalian cells<sup>29</sup> suggest that dedicated E3 ubiquitin ligases functioning in INM-associated protein degradation exist also in metazoans.

**Online Content** Methods, along with any additional Extended Data display items and Source Data, are available in the online version of the paper; references unique to these sections appear only in the online paper.

Received 21 September; accepted 20 November 2014.

1. Mkhail, K. & Moazed, D. The nuclear envelope in genome organization, expression and stability. *Nature Rev. Mol. Cell Biol.* **11**, 317–328 (2010).
2. Zattas, D. & Hochstrasser, M. Ubiquitin-dependent protein degradation at the yeast endoplasmic reticulum and nuclear envelope. *Crit. Rev. Biochem. Mol. Biol.* <http://dx.doi.org/10.3109/10409238.2014.959889> (2014).
3. Ruggiano, A., Foresti, O. & Carvalho, P. Quality control: ER-associated degradation: protein quality control and beyond. *J. Cell Biol.* **204**, 869–879 (2014).
4. Zargari, A. *et al.* Inner nuclear membrane proteins Asi1, Asi2, and Asi3 function in concert to maintain the latent properties of transcription factors Stp1 and Stp2. *J. Biol. Chem.* **282**, 594–605 (2007).
5. Khmelinskii, A. *et al.* Tandem fluorescent protein timers for *in vivo* analysis of protein dynamics. *Nature Biotechnol.* **30**, 708–714 (2012).
6. Deng, M. & Hochstrasser, M. Spatially regulated ubiquitin ligation by an ER/nuclear membrane ligase. *Nature* **443**, 827–831 (2006).
7. Boban, M., Pantazopoulou, M., Schick, A., Ljungdahl, P. O. & Foisner, R. A nuclear ubiquitin-proteasome pathway targets the inner nuclear membrane protein Asi2 for degradation. *J. Cell Sci.* **127**, 3603–3613 (2014).
8. Hu, C.-D., Chinenov, Y. & Kerppola, T. K. Visualization of interactions among bZIP and Rel family proteins in living cells using bimolecular fluorescence complementation. *Mol. Cell* **9**, 789–798 (2002).
9. Forberg, H., Hammar, M., Andréasson, C., Molinér, A. & Ljungdahl, P. O. Suppressors of *ssy1* and *ptr3* null mutations define novel amino acid sensor-independent genes in *Saccharomyces cerevisiae*. *Genetics* **158**, 973–988 (2001).
10. Boban, M. *et al.* Asi1 is an inner nuclear membrane protein that restricts promoter access of two latent transcription factors. *J. Cell Biol.* **173**, 695–707 (2006).
11. Omnis, D. J. & Ljungdahl, P. O. Latency of transcription factor Stp1 depends on a modular regulatory motif that functions as cytoplasmic retention determinant and nuclear degron. *Mol. Biol. Cell* **25**, 3823–3833 (2014).
12. Wienken, C. J., Baaske, P., Rothbauer, U., Braun, D. & Duhr, S. Protein-binding assays in biological liquids using microscale thermophoresis. *Nature Commun.* **1**, 100 (2010).
13. Kostova, Z., Mariano, J., Scholz, S., Koenig, C. & Weissman, A. M. A. Ubc7p-binding domain in Cue1p activates ER-associated protein degradation. *J. Cell Sci.* **122**, 1374–1381 (2009).
14. Biederer, T., Volkwein, C. & Sommer, T. Role of Cue1p in ubiquitination and degradation at the ER surface. *Science* **278**, 1806–1809 (1997).
15. Costanzo, M., Baryshnikova, A., Myers, C. L., Andrews, B. & Boone, C. Charting the genetic interaction map of a cell. *Curr. Opin. Biotechnol.* **22**, 66–74 (2011).
16. Costanzo, M. *et al.* The genetic landscape of a cell. *Science* **327**, 425–431 (2010).
17. Friedlander, R., Jarosch, E., Urban, J., Volkwein, C. & Sommer, T. A regulatory link between ER-associated protein degradation and the unfolded-protein response. *Nature Cell Biol.* **2**, 379–384 (2000).
18. Foresti, O., Rodriguez-Vaejo, V., Funaya, C. & Carvalho, P. Quality control of inner nuclear membrane proteins by the Asi complex. *Science* **346**, 751–755 (2014).
19. Khmelinskii, A., Meurer, M., Duishoev, N., Delhomme, N. & Knop, M. Seamless gene tagging by endonuclease-driven homologous recombination. *PLoS ONE* **6**, e23794 (2011).
20. Baryshnikova, A. *et al.* Synthetic genetic array (SGA) analysis in *Saccharomyces cerevisiae* and *Schizosaccharomyces pombe*. *Methods Enzymol.* **470**, 145–179 (2010).
21. Zattas, D., Adle, D. J., Rubenstein, E. M. & Hochstrasser, M. N-terminal acetylation of the yeast Derlin Der1 is essential for Hrd1 ubiquitin-ligase activity toward luminal ER substrates. *Mol. Biol. Cell* **24**, 890–900 (2013).
22. Uttenweiler, A., Schwarz, H., Neumann, H. & Mayer, A. The vacuolar transporter chaperone (VTC) complex is required for microautophagy. *Mol. Biol. Cell* **18**, 166–175 (2007).
23. Sharpe, H. J., Stevens, T. J. & Munro, S. A comprehensive comparison of transmembrane domains reveals organelle-specific properties. *Cell* **142**, 158–169 (2010).
24. Meinema, A. C., Poolman, B. & Veenhoff, L. M. The transport of integral membrane proteins across the nuclear pore complex. *Nucleus* **3**, 322–329 (2012).
25. Ellenberg, J. *et al.* Nuclear membrane dynamics and reassembly in living cells: targeting of an inner nuclear membrane protein in interphase and mitosis. *J. Cell Biol.* **138**, 1193–1206 (1999).
26. Soullam, B. & Worman, H. J. The amino-terminal domain of the lamin B receptor is a nuclear envelope targeting signal. *J. Cell Biol.* **120**, 1093–1100 (1993).
27. Hinshaw, J. E., Carragher, B. O. & Milligan, R. A. Architecture and design of the nuclear pore complex. *Cell* **69**, 1133–1141 (1992).
28. Beck, M., Lucić, V., Förster, F., Baumeister, W. & Medalia, O. Snapshots of nuclear pore complexes in action captured by cryo-electron tomography. *Nature* **449**, 611–615 (2007).
29. Nakamura, N. The Role of the transmembrane RING finger proteins in cellular and organelle function. *Membranes* **1**, 354–393 (2011).

**Supplementary Information** is available in the online version of the paper.

**Acknowledgements** We thank M. Lemberg, E. Schieberl and B. Bukau for support and discussions, A. Kaufmann, C.-T. Ho, A. Bartosik and B. Besenbeck for help with tFT library construction, K. Ryman for the qRT-PCR analysis of gene expression, M. Hochstrasser for strains, the GeneCore and the media kitchen facilities of the European Molecular Biology Laboratory (EMBL) and Donnelly Centre for support with infrastructure and media. This work was supported by the Sonderforschungsbereich 1036 (SFB1036, TP10) from the Deutsche Forschungsgemeinschaft (DFG) (M.K.), the Swedish Research Council grant VR2011-5925 (P.O.L.), INSERM and grants from ANR (ANR-12-JSV8-0003-001) and Biosit (G.R.), fellowships from the European Molecular Biology Organization (EMBO ALTF 1124-2010 and EMBO ASTF 546-2012) (A.K.) and fellowships from the Ministère de la Recherche et de l'Enseignement Supérieur and La Ligue Contre le Cancer (E.B.). M.K. received funds from the CellNetworks Cluster of Excellence (DFG) for support with tFT library construction. W.H. acknowledges funding from the EC Network of Excellence Systems Microscopy. C.B. was supported by funds from the Canadian Institute for Advanced Research (GNE-BOON-141871), National Institutes of Health (R01HG005853-01), Canadian Institute for Health Research (MOP-102629) and the National Science and Engineering Research Council (RGPIN 204899-6).

**Author Contributions** G.R. designed the BiFC, microscale thermophoresis and ubiquitin pulldown experiments that were performed by E.B., G.L.D. and A.B. M.P., D.J.O. and A.G. contributed the biochemical analysis of Asi-dependent ubiquitylation. M.K. and A.K. designed and coordinated the tFT project. A.K. and M.M. designed and constructed the tFT library and performed the screens with help from D.K. and C.B. B.F. and J.D.B. developed the screen analysis methods, with input from A.K., M.K., W.H. and C.B. M.K., A.K., G.R. and P.O.L. prepared the figures and wrote the paper with input from all authors.

**Author Information** Reprints and permissions information is available at [www.nature.com/reprints](http://www.nature.com/reprints). The authors declare no competing financial interests. Readers are welcome to comment on the online version of the paper. Correspondence and requests for materials should be addressed to M.K. (m.knop@zmbh.uni-heidelberg.de), P.O.L. (per.ljungdahl@su.se) or G.R. (gwenael.rabut@inserm.fr).

## METHODS

**Yeast methods and plasmids.** Yeast genome manipulations (gene deletions and tagging) were performed using PCR targeting, as described<sup>30</sup>. Yeast strains and plasmids used in this study are listed in Supplementary Tables 4 and 5, respectively. **β-galactosidase activity assay.** Cells were grown in synthetic minimal medium and β-galactosidase activity was measured in *N*-lauroyl-sarcosine-permeabilized cells as described<sup>31</sup>.

**RNA isolation and qRT-PCR.** Strains with auxotrophies complemented by plasmids pRS316 (*URA3*), pRS317 (*LYS2*) and pAB1 (*HIS3*, *MET15* and *LEU2*) were grown in synthetic minimal medium to  $10^7$  cells ml<sup>-1</sup> and collected by centrifugation. RNA was isolated using the RiboPure Yeast Kit and treated with Turbo-DNase (Ambion). The quality of RNA preparations was assessed by electrophoresis on a 1% agarose gel with 10 mM guanidine thiocyanate, and the lack of DNA contamination was confirmed by PCR. One microgram of RNA was used for complementary DNA synthesis with oligo (dT)12-19 (Invitrogen) using SuperScript III Reverse Transcriptase (Life Technologies). Quantitative reverse transcriptase PCR (qRT-PCR) reactions were prepared using Kapa SybrFast qPCR Master Mix (Kapa-Biosystems). cDNA mixtures were diluted 1:40 and 5 µl were used in a reaction volume of 20 µl with the following primer pairs: *AGP1*fwd 5'-CTGCCGTGCG TAGGTTT-3' and *AGP1*rev 5'-AGAAGAAGGTGAGATAGCCGA-3'; *GNP1*fwd 5'-CACCACAAGAACAGAACAGAAAC-3' and *GNP1*rev 5'-ACCGACCAG CAAACCAGTA-3'; *TAF10*fwd 5'-ATATTCCAGGATCAGGTCTTCGTTAGC-3' and *TAF10*rev 5'-CAACAACACATCAACAGAATGAGAAGACTAC-3'.

The levels of gene expression in three biological replicates were determined in two separate amplifications with triplicate technical replicates of each of the three genes analysed using the comparative  $\Delta C_T$  method (RotorGene 6000, Corbett Life Science). Relative levels of *AGP1* and *GNP1* messenger RNA were normalized with respect to the levels of the invariant reference gene *TAF10*; the levels of *AGP1* and *GNP1* in strains carrying the indicated mutations were subsequently averaged and normalized to the levels of expression in the corresponding isogenic wild-type strains.

**Purification of decahistidine-ubiquitin protein conjugates.** Ubiquitylated proteins were purified from  $1 \times 10^9$  exponentially growing yeast cells expressing 10×His-tagged ubiquitin using a protocol adapted from ref. 32. Cell pellets were resuspended in 2 ml 20% trichloroacetic acid and lysed for 2 min using glass beads in a Disrupter Genie homogenizer (Scientific Industries). After precipitation, proteins were resuspended in 3 ml guanidium buffer (6 M guanidinium chloride, 100 mM Tris-HCl, pH 9, 300 mM NaCl, 10 mM imidazole, 0.2% Triton X-100 and 5 mM chloroacetamide), clarified at 30,000g and incubated for 1.5 h at room temperature with TALON Metal Affinity Resin (Clontech). The beads were then washed with wash buffer (8 M urea, 100 mM sodium phosphate, pH 7.0, 300 mM NaCl, 5 mM imidazole, 0.2% Triton X-100 and 5 mM chloroacetamide) containing 0.2% SDS (twice) and lacking SDS (twice). 10×His-ubiquitin conjugates were finally eluted with 200 µl elution buffer (8 M urea, 100 mM sodium phosphate, pH 7.0, 300 mM NaCl, 250 mM imidazole, 0.2% Triton X-100 and 5 mM chloroacetamide). Total extracts (1% of the amount used for purification) and ubiquitin conjugate eluates were analysed by SDS-PAGE and immunoblotting with antibodies against the TAP tag (PAP, 1:1,000, Sigma). As controls, levels of ubiquitin conjugates and Pfk1 were assessed with anti-ubiquitin (P4D1 horseradish peroxidase (HRP) conjugate, 1:1,000, Santa Cruz) and anti-Pfk1 antibodies (clone 22C5D8, 1:10,000, Invitrogen), respectively. Immunogenic proteins were detected by chemiluminescence using SuperSignal West Femto Substrate (Thermo Scientific) and recorded using autoradiographic films (CP-BU, Agfa) processed with a Curix 60 developing machine (Agfa).

**Purification of hexahistidine-ubiquitin protein conjugates.** Ubiquitylated proteins were purified from  $5 \times 10^8$  exponentially growing yeast cells expressing 6×His-tagged ubiquitin as previously described<sup>33</sup>. 6×His-ubiquitin conjugates were retained on nickel-nitrilotriacetic acid Sepharose beads (Qiagen) and eluted in the presence of 300 mM (Stp1-HA, Stp1-RI<sub>17-33</sub>-HA) or 500 mM (Stp2-HA, Stp2Δ<sub>2-13</sub>-HA) imidazole. Total extracts, flow-through and eluate fractions were precipitated with 10% trichloroacetic acid, analysed by SDS-PAGE and immunoblotting with antibodies against the haemagglutinin tag (1:5,000, Roche) and the signals were recorded using autoradiographic film (CL-Xposure, Thermo Scientific). As controls, levels of ubiquitin conjugates and Pfk1 were assessed with anti-His<sub>5</sub> (1:5,000, Qiagen) and anti-Pfk1 antibodies (1:10,000, Invitrogen), respectively, and detected by chemiluminescence using SuperSignal West Dura Extended Duration Substrate (Thermo Scientific) and a Molecular Imager ChemiDoc XRS+ with Image Lab v3 build 11 software (BioRad). Loaded total and flow-through fractions correspond to 2% (Stp1-HA or Stp1-RI<sub>17-33</sub>-HA) and 0.7% (Stp2-HA or Stp2Δ<sub>2-13</sub>-HA) of the amount used for purification of ubiquitin conjugates.

**Bimolecular fluorescence complementation.** BiFC interaction assays were performed using E2 and E3 proteins tagged with the VC173 and VN155 fragments (VC and VN) of the Venus fluorescent protein, respectively<sup>34</sup>. All E2 and E3 proteins

were tagged C-terminally, with the following exceptions that were N-terminally tagged: Ubc6, because the C terminus of Ubc6 faces the endoplasmic reticulum lumen<sup>35</sup>; Ubc7, to preserve its interaction with Cue1 (ref. 36); Ubc1, because the growth of strains expressing Ubc1 endogenously tagged at the C terminus with VC appears compromised; the E3 proteins Far1, Mot2, Nam7, Prp19, Ste5 and Tfb3, as they all have their E2 binding domain at the N terminus. All fusions were expressed from their endogenous chromosomal loci, with the exception of Rsp5-VN, which was expressed from its endogenous promoter on the centromeric plasmid pGR703 (Supplementary Table 5).

Strains expressing VC-tagged E2 proteins were constructed in the scEB115 background. scEB115 carries markers for selection of haploid progeny in automated crosses (*can1::STE2pr-spHIS5* and *lyp1::STE3pr-HPH*) and expresses the proteasomal subunit Rpn7 fused to the red fluorescent protein tDimer2 as nuclear marker (Supplementary Table 4). Strains expressing VN-tagged E3 proteins were either obtained from a commercially available collection (Bioneer Corporation) or constructed by homologous recombination in the BY4741 background. Expression of VC- and TAP-tagged fusions was validated by immunoblotting with mouse anti-GFP (clones 7.1 and 13.1, Roche) and peroxidase anti-peroxidase (Sigma) antibodies to detect the VC and TAP tag, respectively, and mouse anti-actin (clone c4, Merck Millipore) for loading controls.

Strains expressing individual E2 and E3 protein fusions were crossed to produce an array of yeast strains each expressing Rpn7-tDimer2 and a unique combination of tagged E2 and E3 proteins, as described<sup>20</sup>. The resulting strains were cultivated overnight at 20 °C in YPD medium and diluted in low fluorescence medium<sup>37</sup> 3–4 h before imaging. Imaging was performed in 8-well LabTek chambers or 96-well plates (Imaging plates CG, Zell-Kontakt) using an inverted Leica SP8 confocal microscope. Images of the BiFC signal were collected using a 514 nm laser and a narrow band-pass filter (525–538 nm) around the emission peak of the Venus fluorescent protein to reduce the contribution of cellular autofluorescence. Rpn7-tDimer2 was imaged simultaneously using a 580–630 nm filter. Cellular autofluorescence was imaged separately using the same band-pass filter as for BiFC images, but with a 458 nm excitation. Rpn7 localizes to the nucleus throughout the cell cycle in growing cells and relocates to cytoplasmic structures when cells enter quiescence<sup>38</sup>. Rpn7-tDimer2 images were visually inspected before image processing to verify that cells are not quiescent. Rpn7-tDimer2 and autofluorescence images were used to segment the BiFC images into nuclear and cytoplasmic (whole cell minus nucleus) regions and to unmix the BiFC signal. Image segmentation and single-cell fluorescence measurements were performed using custom plugins in ImageJ<sup>39</sup> (available on request). To enable comparison of data from different experiments, the quantification results were rescaled so that BiFC signals of control cells had a mean of zero and a standard deviation of one. Statistical analysis and graphical representation were performed with GraphPad Prism software. Statistically significant differences from control cells were identified by one-way ANOVA followed by Bonferroni post-hoc tests to correct for multiple comparisons. No statistical method was used to predetermine sample size.

**Recombinant protein expression and purification.** *Escherichia coli* BL21(DE3) were transformed with plasmids encoding MBP-Hrd1<sup>CT</sup> (Hrd1 residues 321–551), MBP-Asi1<sup>RING</sup> (Asi1 residues 559–624), MBP-Asi3<sup>RING</sup> (Asi3 residues 613–676), glutathione S-transferase (GST)-Ubc6<sup>ATM</sup> (Ubc6 residues 1–230), GST-Ubc7 or Cue1<sup>U7BR</sup> (Cue1 residues 151–203) and were cultivated in LB medium. Cue1<sup>U7BR</sup> was coexpressed with GST-Ubc7. Protein expression was induced by addition of 1 mM isopropyl-β-D-thiogalactoside (IPTG) during 4 h at 25 °C. Cells were pelleted, resuspended in PBS, and lysed by sonication. Lysates were rotated with glutathione (GE Healthcare) or amylose beads (New England Biolab) for 1 h at 4 °C. Beads were washed with PBS containing 1 mM dithiothreitol (DTT). E2s were cleaved from GST using thrombin (Stago). MBP-E3s were eluted using 10 mM amylose and dialysed against PBS plus 1 mM DTT. All recombinant proteins were concentrated using spin filters (3 kDa, Amicon). Protein purity was tested by Coomassie staining after SDS-PAGE. Protein concentration was estimated by absorbance at 280 nm.

**Microscale thermophoresis.** Microscale thermophoresis analysis was performed essentially as described<sup>12</sup> using MBP-Asi1<sup>RING</sup>, MBP-Asi3<sup>RING</sup> or MBP-Hrd1<sup>CT</sup> fluorescently labelled with the fluorescent dye NT-647 (labelling was performed with the Monolith Protein Labelling Kit RED-NHS according to the instructions of the supplier) and high precision standard treated capillaries. MBP-E3s were diluted to 100 nM in PBS, 5% glycerol, 0.1% Tween 20, 1 mM DTT, 10 µM ZnAc and titrated with varying concentrations of unlabelled E2s before loading into capillaries. The difference of the thermophoretic properties of MBP-E3s were measured using a Monolith NT.115 instrument (NanoTemper Technologies GmbH) and a laser power of 60%. A nonlinear fit with the law of mass action was used to derive the dissociation constant ( $K_d$ ) of the interaction as well as the theoretical thermophoretic properties of the MBP-E3 in its fully bound and unbound states. Those values were then used to normalize the measurements and calculate the

fraction of E3 bound at each E2 concentration. Data were plotted and fitted with the GraphPad Prism software.

**tFT library construction.** A total of 4,081 verified or uncharacterized *S. cerevisiae* open reading frames were selected for tagging based on structural and functional criteria (detailed in Supplementary Methods) to increase the probability that the C-terminal tFT tag would not affect protein functionality, and to avoid exposing the tag to an environment that could affect folding and maturation of the fluorescent proteins. Protocols for strain construction and validation are described in the Supplementary Methods. In brief, strain manipulations were automated and performed in 96-well format whenever possible. Using PCR targeting<sup>30</sup> and lithium acetate transformation of yeast<sup>40</sup>, the module for seamless protein tagging with the mCherry-sfGFP timer (pMaM168 in Supplementary Table 5) was integrated into each selected genomic locus in the strain yMaM330 (Supplementary Table 4), a strain compatible with automated yeast genetics that carried a construct for conditional expression of the I-SceI meganuclease from the *GAL1* promoter integrated into the *leu2* locus. Correct integration of the tagging module into each locus and expression of tFT protein fusions was verified by PCR and whole colony fluorescence measurements for 4,044 open reading frames, with two independent clones validated for 3,952 open reading frames (Supplementary Table 2).

**tFT library screening.** Haploid array strains carrying deletions of individual components of the ubiquitin–proteasome system were obtained from the genome-wide heterozygous diploid yeast deletion library<sup>41</sup> by sporulation and tetrad dissection. Screens were conducted in 1536-colony format. Using pinning robots (BioMatrix, S&P Robotics), tFT query strains (before marker excision) were mated with array mutants. Selection of diploids, sporulation and selection of haploids carrying simultaneously a tFT protein fusion and a gene deletion were performed by sequential pinning on appropriate selective media, as described<sup>20</sup>, followed by seamless marker excision<sup>19</sup>. In each screen, a single tFT strain was crossed to a set of mutants in the ubiquitin–proteasome pathway (including the *asi1Δ*, *asi3Δ*, *hrd1Δ*, *doa10Δ*, *ubc6Δ* and *ubc7Δ* mutants) (A.K. *et al.*, manuscript in preparation) with four technical replicates of each cross. Technical replicates were arranged next to each other. Fluorescence intensities of the final colonies were measured after 24 h of growth on synthetic complete medium lacking histidine at 30 °C using Infinite M1000 or Infinite M1000 Pro plate readers equipped with stackers for automated plate loading (Tecan) and custom temperature control chambers. Measurements in mCherry (587/10 nm excitation, 610/10 nm emission, optimal detector gain) and sfGFP (488/10 nm excitation, 510/10 nm emission, optimal detector gain) channels were performed at 400 Hz frequency of the flash lamp, with ten flashes averaged for each measurement.

Measurements were filtered for potentially failed crosses based on colony size after haploid selection. Fluorescence intensity measurements were log-transformed and the data were normalized for spatial effects on plates by local regression. To estimate the changes from normal protein stability, median effects for tFT and deletion strains were subtracted from log-ratios of mCherry and sfGFP intensities. To avoid variance-mean dependences, standard deviations were regressed against the absolute fluorescence intensities. Changes in protein stability were divided by the regressed standard deviations, yielding a measurement comparable to a *z*-score, and tested against the hypothesis of zero change. A moderated *t*-test implemented in the R/Bioconductor package limma<sup>42</sup> was used to compute *P* values. *P* values were adjusted for multiple testing by controlling the false discovery rate using the method of Benjamini–Hochberg.

Crosses with additional mutants were performed with independently constructed deletion strains using identical procedures on a RoToR pinning robot (Singer). Whole colony fluorescence intensities were corrected for autofluorescence using measurements of corresponding mutant colonies crossed to strain yMaM344-2 (Supplementary Table 4) expressing a truncated non-fluorescent mCherry<sup>AN</sup> protein. For each tFT fusion, mCherry/sfGFP intensity ratios in each mutant were compared to a control cross with a wild-type strain carrying the *kanMX* selection marker in the *his3Δ* locus.

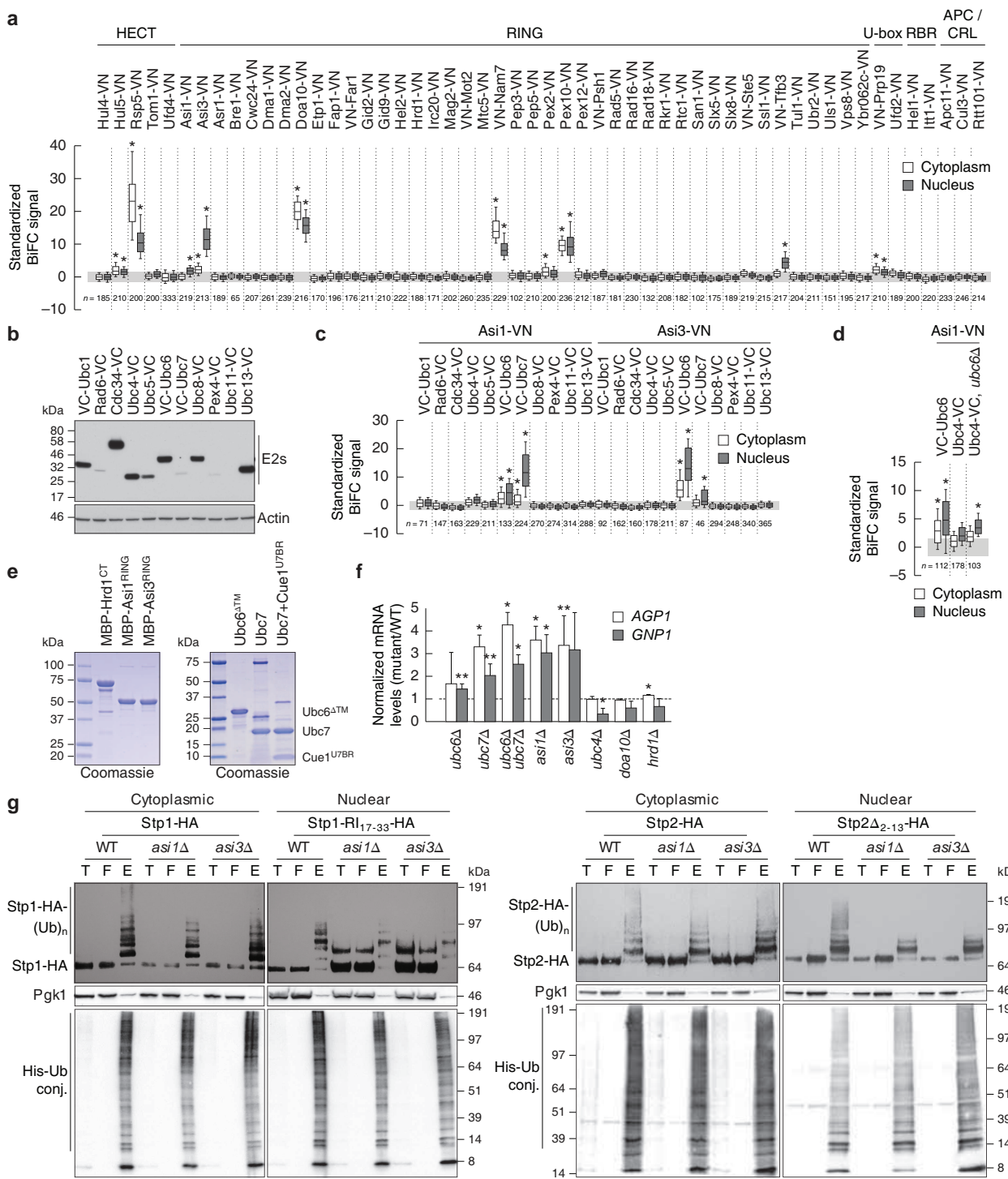
**Fluorescence microscopy.** Strains were grown at 30 °C in low fluorescence medium (synthetic complete medium prepared with yeast nitrogen base lacking folic acid and riboflavin; CYN6501, ForMedium) to 0.4–1.2 × 10<sup>7</sup> cells ml<sup>-1</sup> and attached

to glass-bottom 96-well plates (MGB096-1-2-LG-L, Matrical) using Concanavalin A (C7275, Sigma) as described<sup>43</sup>. Single plane images were acquired on a DeltaVision Elite system (Applied Precision) consisting of an inverted epifluorescence microscope (IX71; Olympus) equipped with an LED light engine (SpectraX, Lumencor), 475/28 and 575/25 nm excitation, and 525/50 and 624/40 nm emission filters (Semrock), a dual-band beam splitter 89021 (Chroma Technology), using either a 100× numerical aperture (NA) 1.4 UPlanSApo or a 60× NA 1.42 PlanApoN oil immersion objective (Olympus), an sCMOS camera (pco.edge 4.2, PCO) and a motorized stage contained in a temperature-controlled chamber. Image correction and quantification were performed in ImageJ<sup>39</sup>. Dark signal and flat field corrections were applied to all images as described<sup>43</sup>. Image deconvolution was performed with Softworx software (Applied Precision) using the conservative ratio algorithm with default parameter settings. Individual cell, perinuclear region and cytoplasm segmentation masks were manually defined in deconvolved images and applied to non-deconvolved images. Mean single-cell fluorescence measurements were corrected for cellular autofluorescence. Mean perinuclear fluorescence measurements were corrected for cytoplasmic fluorescence of each individual cell.

Strains expressing N- and C-terminally tagged Vtc1 and Vtc4 were imaged with exposure setting adjusted to the expression levels: 3.3-fold longer exposure time for C-terminally tagged fusions. Representative deconvolved images were scaled identically.

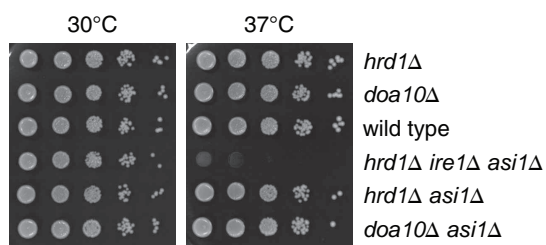
**Cycloheximide chases.** Strains were grown at 30 °C in synthetic complete medium to ~0.8 × 10<sup>7</sup> cells ml<sup>-1</sup> density before addition of cycloheximide to 100 µg ml<sup>-1</sup> final concentration. One-millilitre samples taken at each time point were immediately mixed with 150 µl of 1.85 M NaOH and 10 µl β-mercaptoethanol, and flash frozen in liquid nitrogen. Whole-cell extracts were prepared as previously described<sup>40</sup>, separated by SDS-PAGE followed by semi-dry blotting and probed sequentially with mouse anti-HA (12CA5) and mouse anti-Pgk1 (22C5D8, Molecular Probes) antibodies. A secondary goat anti-mouse antibody (IgG (H+L)-HRP, Dianova) was used for detection on a LAS-4000 system (Fuji).

30. Janke, C. *et al.* A versatile toolbox for PCR-based tagging of yeast genes: new fluorescent proteins, more markers and promoter substitution cassettes. *Yeast* **21**, 947–962 (2004).
31. Andréasson, C. & Ljungdahl, P. O. The N-terminal regulatory domain of Stp1p is modular and, fused to an artificial transcription factor, confers full Ssy1p-Ptr3p-Ssy5p sensor control. *Mol. Cell. Biol.* **24**, 7503–7513 (2004).
32. Becuwe, M. *et al.* A molecular switch on an arrestin-like protein relays glucose signaling to transporter endocytosis. *J. Cell Biol.* **196**, 247–259 (2012).
33. Léon, S., Erpapazoglou, Z. & Haguenuer-Tsapis, R. Ear1p and Ssh4p are new adaptors of the ubiquitin ligase Rsp5p for cargo ubiquitylation and sorting at multivesicular bodies. *Mol. Biol. Cell* **19**, 2379–2388 (2008).
34. Shyu, Y. J., Liu, H., Deng, X. & Hu, C. Identification of new fluorescent protein fragments for biomolecular fluorescence complementation analysis under physiological conditions. *Biotechniques* **40**, 61 (2006).
35. Sommer, T. & Jentsch, S. A protein translocation defect linked to ubiquitin conjugation at the endoplasmic reticulum. *Nature* **365**, 176–179 (1993).
36. Metzger, M. B. *et al.* A structurally unique E2-binding domain activates ubiquitination by the ERAD E2, Ubc7p, through multiple mechanisms. *Mol. Cell* **50**, 516–527 (2013).
37. Sheff, M. A. & Thorn, K. S. Optimized cassettes for fluorescent protein tagging in *Saccharomyces cerevisiae*. *Yeast* **21**, 661–670 (2004).
38. Laporte, D., Salin, B., Daignan-Fornier, B. & Sagot, I. Reversible cytoplasmic localization of the proteasome in quiescent yeast cells. *J. Cell Biol.* **181**, 737–745 (2008).
39. Schneider, C. A., Rasband, W. S. & Eliceiri, K. W. NIH Image to ImageJ: 25 years of image analysis. *Nature Methods* **9**, 671–675 (2012).
40. Knop, M. *et al.* Epitope tagging of yeast genes using a PCR-based strategy: more tags and improved practical routines. *Yeast* **15**, 963–972 (1999).
41. Winzeler, E. A. *et al.* Functional characterization of the *S. cerevisiae* genome by gene deletion and parallel analysis. *Science* **285**, 901–906 (1999).
42. Smyth, G. K. in *Bioinformatics and Computational Biology Solutions Using R and Bioconductor* (eds Gentleman, R., Carey, V., Dudoit, S., Irizarry, R. & Huber, W.) 397–420 (Springer, 2005).
43. Khmelinskii, A. & Knop, M. Analysis of protein dynamics with tandem fluorescent protein timers. *Methods Mol. Biol.* **1174**, 195–210 (2014).

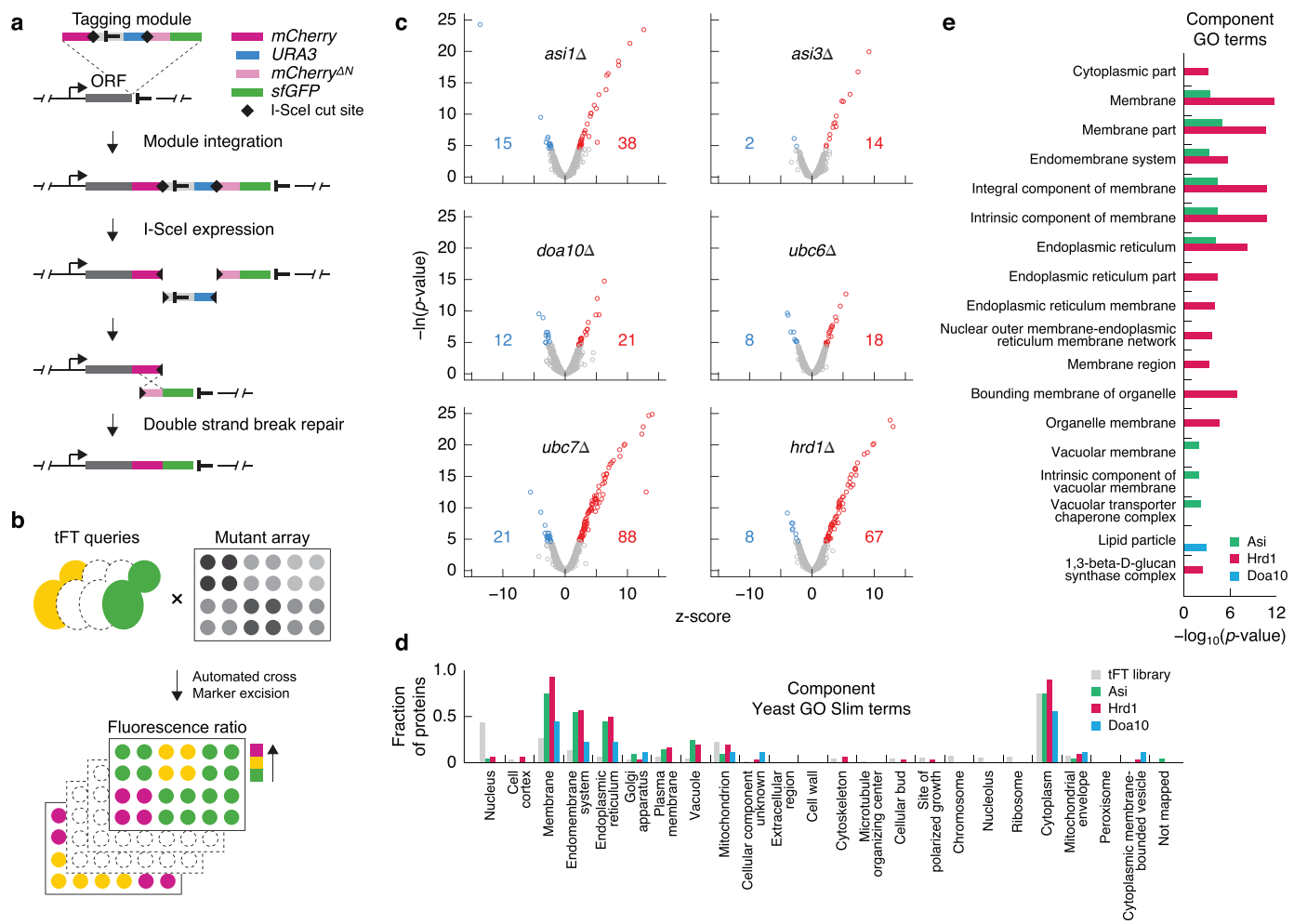


**Extended Data Figure 1 | Identification of Ubc6 and Ubc7 ubiquitin-conjugating enzymes as functional interacting partners of Asi1 and Asi3.**  
**a**, Quantification of BiFC signals in cells expressing VC–Ubc6 and all tested E3 ubiquitin ligases. BiFC signals were measured in the cytoplasm and nucleus of individual cells ( $n$  as shown). Whiskers extend from the tenth to the ninetieth percentiles. The same representation is used in **c** and **d**. **b**, Immunoblot showing expression levels of VC-tagged E2 ubiquitin-conjugating enzymes. Ubc11–VC could not be detected in the growth condition of the BiFC assay. **c**, Quantification of BiFC signals in cells co-expressing VC-tagged E2 ubiquitin-conjugating enzymes and Asi1–VN or Asi3–VN ( $n$  as shown). **d**, Detection of a significant BiFC signal between Asi1–VN and Ubc4–VC in cells lacking UBC6 ( $n$  as shown). **e**, Coomassie-stained gels of recombinant proteins used in microscale thermophoresis experiments. **f**, mRNA levels of *AGP1* and *GNP1* measured with qRT–PCR in the indicated strains (mean  $\pm$  s.d.,  $n$  = 3 clones).

The signal was normalized to wild type (dashed line). g, Ubiquitylation of Stp1-HA or Stp1-RI<sub>17-33</sub>-HA (Stp1 variant in which amino acid residues 2-64 were replaced with Stp1 residues 17-33 flanked by minimal linker sequences) (left) and Stp2-HA or Stp2Δ<sub>2-13</sub>-HA (Stp2 variant lacking amino acid residues 2-13) (right) in strains expressing 6×His-ubiquitin. Stp1-RI<sub>17-33</sub> and Stp2Δ<sub>2-13</sub> variants exhibit compromised cytoplasmic retention and enhanced Asi-dependent degradation, whereas full-length Stp1 is degraded primarily in the cytoplasm in a SCF<sup>Grr1</sup>-dependent manner<sup>11</sup>. Total cell extracts (T), flow-through (F) and ubiquitin conjugates (E) eluted after immobilized-metal affinity chromatography were separated by SDS-PAGE followed by immunoblotting with antibodies against the HA-tag, Pgk1 and the His-tag. Representative immunoblots from three technical replicates. \* $P < 10^{-4}$  (a, c and d; one-way ANOVA with Bonferroni correction for multiple testing), and \* $P < 0.05$ , \*\* $P < 0.1$  (f; two-tailed *t*-test).

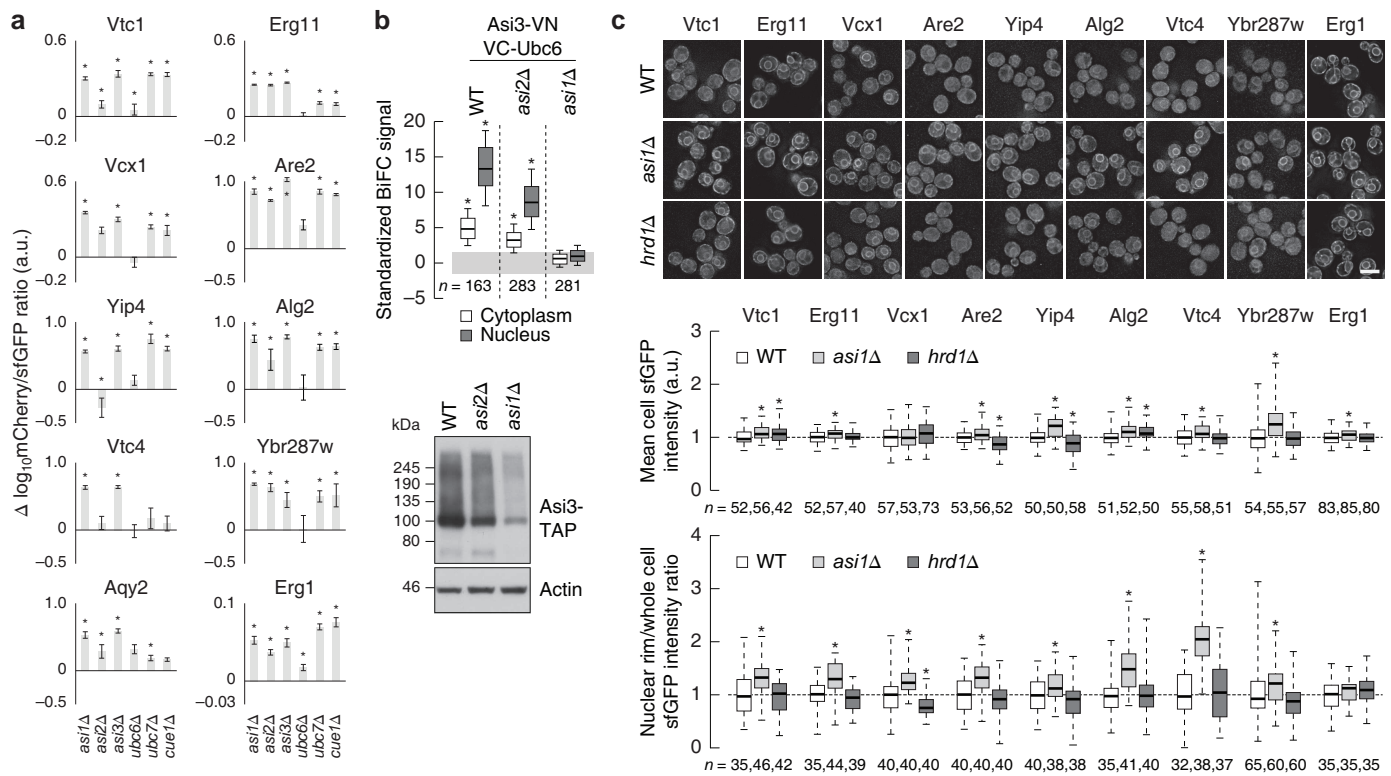


Extended Data Figure 2 | Lack of genetic interaction between *ASII* and *HRD1* or *DOA10* at 37 °C. Tenfold serial dilutions of strains grown on synthetic complete medium for 2 days at 30 or 37 °C.



**Extended Data Figure 3 | tFT screens for substrates of Asi and ERAD E3 ubiquitin ligases.** **a**, Tagging approach used to construct the tFT library in a strain carrying the I-SceI meganuclease under an inducible promoter. First, a module for seamless C-terminal protein tagging with the mCherry-sfGFP timer is integrated into a genomic locus of interest using conventional PCR targeting. Subsequent I-SceI expression leads to excision of the heterologous terminator and the URA3 selection marker, followed by repair of the double-strand break by homologous recombination between the mCherry and mCherry<sup>AN</sup> sequences. A tFT fusion protein is expressed under control of endogenous promoter and terminator in the final strain. **b**, Workflow of screens for substrates of E3 ubiquitin ligases involved in protein degradation. Each tFT query strain is crossed to an array of mutants carrying different gene

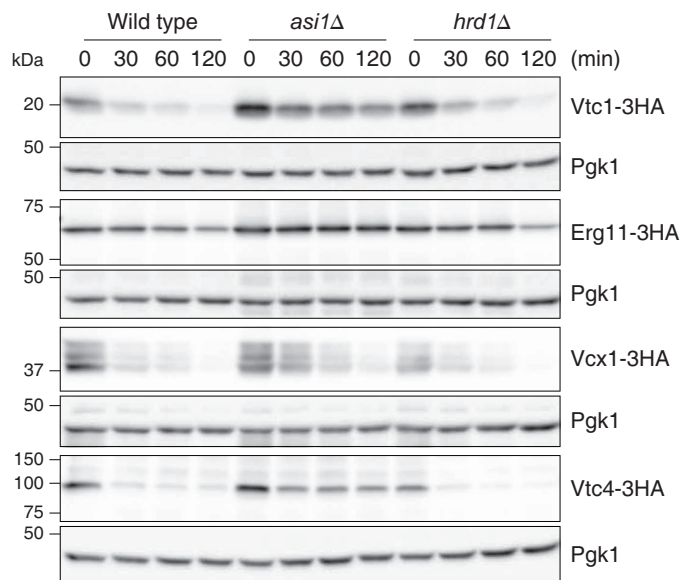
deletion alleles. The resulting strains are imaged with a fluorescence plate reader to identify proteins with altered stability in each mutant. **c**, Volcano plots of the screens for proteins with altered stability in the indicated mutants. Plots show z-scores for changes in protein stability on the x axis and the negative logarithm of  $P$  values adjusted for multiple testing on the y axis. The number of proteins with increased (red) or decreased (blue) stability at 1% false discovery rate is indicated. **d**, Fraction of proteins in the tFT library and in the three clusters in Fig. 3b mapped to the full yeast slim set of component GO terms. Note that the GO term cytoplasm contains all cellular contents except the nucleus and the plasma membrane. **e**, The three clusters in Fig. 3b are enriched for proteins in the indicated component GO terms. Bar plot shows  $-\log_{10}$ -transformed  $P$  values of significant enrichments.



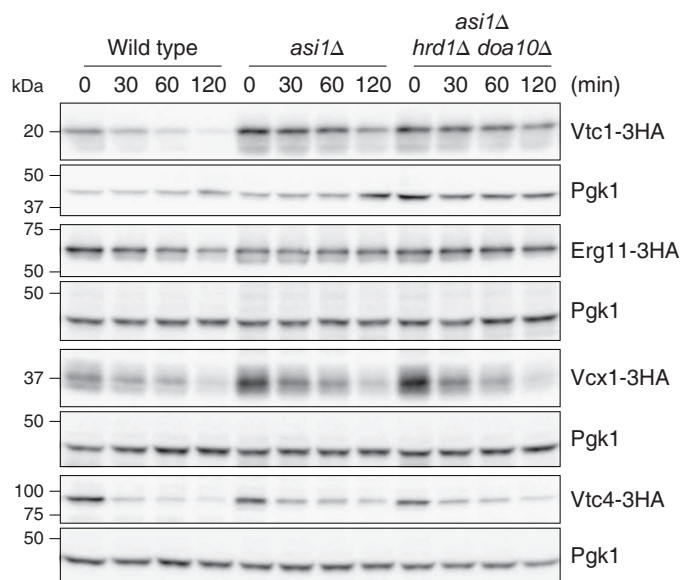
**Extended Data Figure 4 | Analysis of integral membrane protein substrates of the Asi E3 ubiquitin ligase.** **a**, Differences in the  $\log_{10}$  mCherry/sfGFP intensity ratio between the indicated mutants and the wild type (mean  $\pm$  s.d.,  $n = 4$ ) for tFT-tagged proteins from the Asi cluster in Fig. 3b. **b**, Quantification of BiFC signals in strains co-expressing VC-Ubc6 and Asi3-VN (top). BiFC signals were measured in the cytoplasm and nucleus of individual cells ( $n$  as shown). Whiskers extend from tenth to ninetieth percentiles. A substantial BiFC signal is retained in the *asi2Δ* mutant, despite reduced expression of Asi3

(immunoblot, bottom). **c**, Quantification of sfGFP signals in strains expressing tFT-tagged proteins from the Asi cluster in Fig. 3b. Fluorescence microscopy examples representative of five fields of view (top). Scale bar, 5  $\mu$ m. sfGFP intensities were measured in individual cells (middle) and at the nuclear rim (bottom). For each protein, measurements were normalized to the mean of the respective wild type. Whiskers extend from minimum to maximum values.

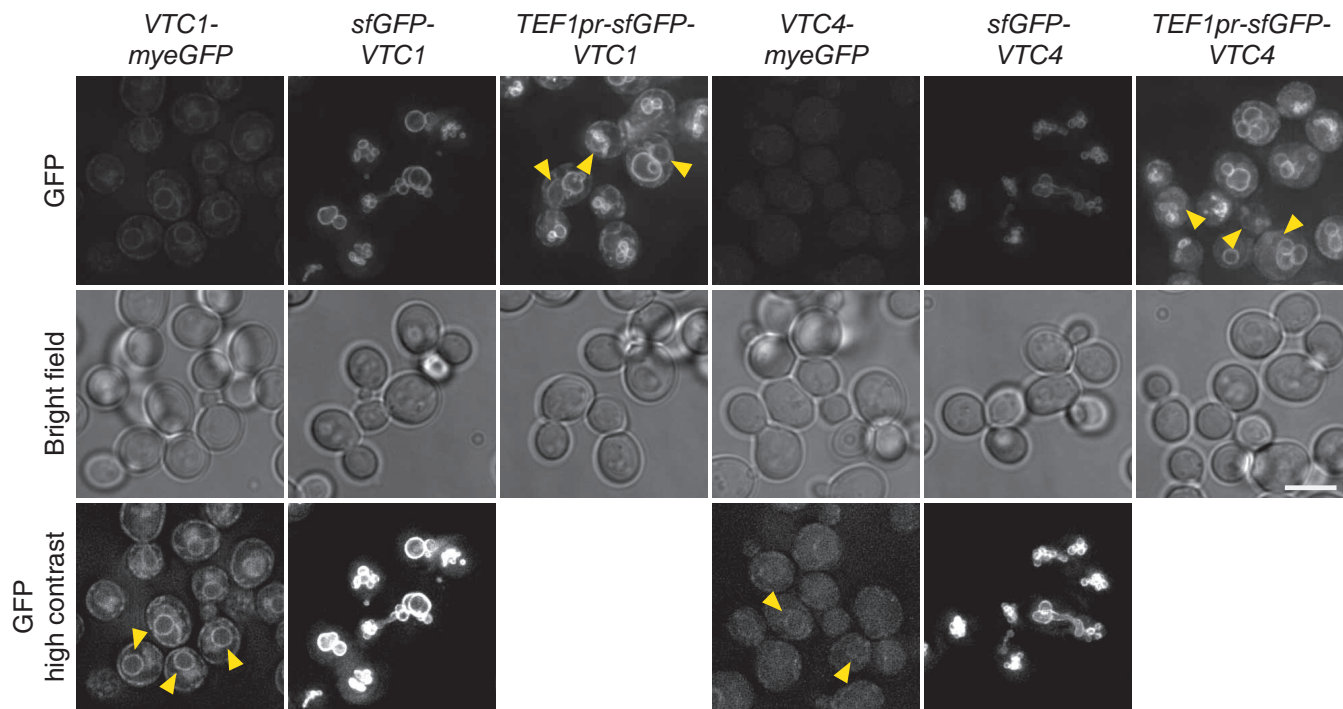
\* $P < 0.05$  (**a** and **c**; two-tailed  $t$ -test) and \* $P < 10^{-4}$  (**b**; one-way ANOVA with Bonferroni correction for multiple testing).



**Extended Data Figure 5 | Cycloheximide chase experiments with substrates of the Asi E3 ubiquitin ligase.** Degradation of 3×HA-tagged proteins after blocking translation with cycloheximide. Whole-cell extracts were separated by



SDS-PAGE followed by immunoblotting with antibodies against the HA tag and Pgk1 as loading control. Representative immunoblots from two technical replicates. Left, wild-type and *asi1Δ* immunoblots are reproduced in Fig. 3f.



**Extended Data Figure 6 | Influence of tagging and expression levels on localization of Vtc1 and Vtc4.** Fluorescence microscopy of strains expressing Vtc1 or Vtc4 tagged endogenously with monomeric yeast codon-optimized enhanced GFP (myeGFP) at the C terminus or tagged with sfGFP at the N

terminus and expressed under control of endogenous or *TEF1* promoters. Representative deconvolved images of five fields of view with ~100 cells each. Arrowheads indicate nuclear rim localization. Scale bar, 5  $\mu$ m.